

**Under-ice acoustic navigation using real-time model-aided range estimation**

EeShan C. Bhatt,<sup>1, 2, a</sup> Oscar Viquez,<sup>2</sup> and Henrik Schmidt<sup>2</sup>

<sup>1</sup>*MIT-WHOI Joint Program in Oceanography/Applied Ocean Science & Engineering,  
Cambridge and Woods Hole, MA, USA*

<sup>2</sup>*Department of Mechanical Engineering, Massachusetts Institute of Technology,  
Cambridge, MA*

(Dated: 20 February 2022)

1 The long baseline (LBL) underwater navigation paradigm relies on the conversion  
2 of recorded travel time to range to trilaterate for position. For real-time opera-  
3 tions, this conversion has assumed an isovelocity sound speed. For re-navigation  
4 in post-processing, computationally and/or labor intensive acoustic modeling may  
5 be employed to reduce uncertainty driven by multipath arrivals. This work demon-  
6 strates a real-time ray-based prediction method of the effective sound speed along  
7 a path from source to receiver to minimize vehicle position error. This method was  
8 implemented for a small scale AUV-LBL system in March 2020, in the Beaufort Sea,  
9 in total ice-covered conditions and a double ducted acoustic propagation environ-  
10 ment. The vehicle was successfully deployed and recovered. Given the lack of GPS  
11 data throughout the vehicle's mission, however, the pseudorange performance is first  
12 evaluated on connections between GPS-linked beacons. The real-time ranging error  
13 between beacons is roughly 11 meters at distances up to 3 km. But a consistent over-  
14 estimation in the real-time method, the Minimum Bounce Criteria (MBC), provides  
15 insights for improved eigenray filtering, which we call the Nearest Bounce Criteria  
16 (NBC). An operationally equivalent pipeline is used to re-position the LBL bea-  
17 cons and re-navigate the AUV, using a modeled, historical, and a locally observed  
18 sound speed profile. The median re-positioning errors for the MBC and NBC are  
19 roughly 10 and 3 meters, respectively. The improved trilateration performance for  
20 re-positioning and re-navigation suggests that this approach effectively extends the  
21 single meter accuracy of the deployed GNSS units into the water column.

---

<sup>a</sup>[ebhatt@whoi.edu](mailto:ebhatt@whoi.edu)

<sup>22</sup> **I. INTRODUCTION**

<sup>23</sup> Autonomous underwater vehicles (AUVs) are increasingly capable platforms to explore  
<sup>24</sup> and sample the ocean, particularly for remote and/or dangerous regions. However, navi-  
<sup>25</sup> gation uncertainty is a major challenge in considering AUVs as standard tools for oceano-  
<sup>26</sup> graphic research. While land and air-based robots utilize information from Global Naviga-  
<sup>27</sup> tion Satellite Systems (GNSS) to achieve stunning location accuracy and precision through-  
<sup>28</sup> out the duration of their missions, AUVs cannot access GNSS while underwater due to  
<sup>29</sup> the rapid attenuation of electromagnetic waves. Therefore, underwater vehicles have relied  
<sup>30</sup> on any combination of dead reckoning, hydrodynamic models, inertial navigation systems,  
<sup>31</sup> doppler velocity logs, and acoustic baseline positioning systems for navigation ([Paull \*et al.\*, 2014](#)). Limiting navigation error and drift requires an AUV to periodically stall on the  
<sup>32</sup> surface and obtain a GNSS fix to reset its position error. This foolproof method of self-  
<sup>33</sup> positioning is undesirable for stealth, adverse weather conditions, and mission efficiency,  
<sup>34</sup> and inaccessible in a GNSS-denied situation like an ice-covered environment.  
<sup>35</sup>

<sup>36</sup> Of underwater acoustic navigation systems, long baseline (LBL) is the most GPS-like in  
<sup>37</sup> style and scale, and most appropriate for mitigating drift without overburdening computa-  
<sup>38</sup> tion or payload size on the vehicle ([Paull \*et al.\*, 2014; Van Uffelen, 2021](#)). The state-of-the-art  
<sup>39</sup> for LBL outsources depth to a pressure sensor and solves the two-dimensional localization  
<sup>40</sup> problem with an isovelocity, linear scaling between one way travel time (OWTT) and range  
<sup>41</sup> ([Eustice \*et al.\*, 2006, 2007; Webster \*et al.\*, 2009, 2012](#)). This assumption is valid for short  
<sup>42</sup> scale operations but oversimplifies propagation for larger and/or complex acoustic environ-

43 ments. To achieve single meter, GNSS-like performance in a GNSS-denied environment, we  
44 demonstrate an embedded ray-based data processing algorithm to convert recorded OWTTs  
45 into pseudorange estimates. This methodology was integrated onto the AUV Macrura, de-  
46 ployed and recovered in the Beaufort Sea, in March 2020, during the Ice Exercise 2020  
47 (ICEX20). A physics-driven methodology that received an *in situ* sound speed profile (SSP)  
48 was necessary despite the small operational domain because of the relatively high-risk mis-  
49 sion environment—total under-ice conditions and a variable double ducted acoustic environ-  
50 ment.

51 For clarity, we delineate specific definitions for timing, positioning, and navigation from  
52 [Howe \*et al.\* \(2019\)](#).

53 1. Timing is the ability to acquire and maintain accurate and precise time anywhere in  
54 the domain of interest within user-defined timeliness parameters

55 2. Positioning is the ability to accurately and precisely determine one's location refer-  
56 enced to a standard geodetic system

57 3. Navigation is the ability to determine current and desired position (relative or absolute)  
58 and apply corrections to course, orientation, and speed to attain a desired position  
59 anywhere in the domain of concern

60 Thus, navigation is inherently in real time and depends on positioning; positioning depends  
61 on timing. We also suggest re-navigation and re-positioning as post-processed corollaries,  
62 which may include knowledge or processing capabilities not available *in situ*.

63 While RAFOS floats championed one way ranging for re-positioning (Duda *et al.*, 2006;  
 64 Rossby *et al.*, 1986), the ability to do so for navigation was facilitated by the advent of  
 65 the WHOI Micro-Modem (Singh *et al.*, 2006) and synchronized chip scale atomic clocks  
 66 (Gardner and Collins, 2016). AUV navigation efforts have achieved root mean square (RMS)  
 67 localization error on the order of tens of meters relative to GNSS surface position over less  
 68 than ten kilometers in shallow (Claus *et al.*, 2018; Eustice *et al.*, 2007; Kepper *et al.*, 2017)  
 69 and deep water (Jakuba *et al.*, 2008; Kunz *et al.*, 2008b; Webster *et al.*, 2009). However,  
 70 these efforts all used a nominal sound speed for travel time conversion and the vehicles were  
 71 limited to shallower isovelocity regimes.

72 Localization algorithms that do consider environmental or acoustic uncertainty tend to  
 73 focus on longer and larger experiments, where spatio-temporal variability cannot be ignored.  
 74 These methods have been reserved for post-processing as they can be labor intensive, com-  
 75 putationally heavy, and/or require additional information like contemporaneous data. For  
 76 example, gliders navigating with kinematic flight models and equipped with acoustic modems  
 77 were later unambiguously associated with predicted ray arrivals, resulting in roughly a kilo-  
 78 meter error and hundred meters uncertainty over basin scale propagation (Van Uffelen *et al.*,  
 79 2013). A follow up study investigated how a single temporally and spatially averaged SSP  
 80 could mitigate position error for a four month glider mission (Van Uffelen *et al.*, 2016). Wu  
 81 *et al.* (2018) cross correlate three days of real acoustic records with synthetic ones generated  
 82 through ocean model snapshots from HYCOM (Chassagnet *et al.*, 2007). While potentially  
 83 applicable for various ocean states, this is reliant on model realism and impractical for real-  
 84 time operations. Mikhalevsky *et al.* (2020) introduces a “cold start” algorithm that does not

85 require prior knowledge of track, position, or sound speed information. The algorithm inputs  
86 a four-dimensional ocean model, constrained by tomography data, into a range dependent  
87 ray code to isolate the last path detected in a full multipath pattern. Then, a representative  
88 group speed is solved for alongside position in a least squares fashion. This approach is able  
89 to re-position a floating hydrophone array with an error of 58 m and a standard deviation  
90 of 32 m based on six sources 129–450 km away but remains to be seen for real-time navigation.

91 The ICEX20 AUV deployment necessitated an environmentally- and physically-driven  
92 relationship between recorded travel time and estimated range due to the multipath uncer-  
93 tainty brought upon by an increasingly observed double ducted environment in the Beaufort  
94 Sea, which some refer to as the “Beaufort Lens” (Chen *et al.*, 2019; Chen and Schmidt,  
95 2020; Litvak, 2015).

96 Given that a lens introduces significant ray refraction, the Beaufort Lens is a convenient  
97 shorthand for the spatio-temporal variability of the local temperature and sound speed  
98 maxima generally around 50 to 60 m in depth. A neutrally buoyant layer of warm Pacific  
99 Summer Water creates a unique double ducted environment —the upper duct degrades  
100 signal coherence due to intensified ice interaction and the lower duct effectively traps sound  
101 for long range propagation (Poulsen and Schmidt, 2016a). Modeling output (Duda *et al.*,  
102 2021, 2019) and experimental observations (Ballard *et al.*, 2020; Bhatt, 2021) suggest the  
103 duct is persistent and widespread but not necessarily continuous; it and its acoustic effects  
104 can be non-existent, minimal, or drastic. Transmissions in the upper duct, between the  
105 surface ice and the lens, experience minimal attenuation but degrade in signal coherence  
106 with repeated reflections under the ice. In lower duct, between the lens and its conjugate

<sup>107</sup> depth in the Atlantic water, roughly 200 m, sound above 350 Hz is trapped effectively for  
<sup>108</sup> long range propagation (Poulsen and Schmidt, 2016b).

<sup>109</sup> Thorough reviews of uncrewed vehicle operations in polar environments can be found in  
<sup>110</sup> (Norgren *et al.*, 2014) and (Barker *et al.*, 2020); there is no comparable work in the Arctic  
<sup>111</sup> for a short range AUV deployment in the Beaufort Lens. Seminal (Bellingham *et al.*, 1995;  
<sup>112</sup> Brooke, 1981; Hayes and Morison, 2002; Jackson, 1983; Light and Morison, 1989) and more  
<sup>113</sup> recent AUV deployments (Fossum *et al.*, 2021; Jakuba *et al.*, 2008; Kukulya *et al.*, 2010;  
<sup>114</sup> Kunz *et al.*, 2008a; Plueddemann *et al.*, 2012; Timmermans and Winsor, 2013) witnessed the  
<sup>115</sup> classical upward refracting sound speed profile that is amenable to an isovelocity assumption.

<sup>116</sup> Of note, despite different platforms and scales, are recent glider deployments in the  
<sup>117</sup> Canada Basin. In 2014, in partially ice-covered conditions, a long range LBL system with  
<sup>118</sup> WHOI Micro-Modems at 100 m exploited the lower duct for long range communication with  
<sup>119</sup> two gliders (Freitag *et al.*, 2015; Webster *et al.*, 2015). The sound speed value measured at  
<sup>120</sup> the time of reception was used to estimate range in post-processing. The beacon-to-beacon  
<sup>121</sup> performance was excellent, achieving contact at ranges greater than 200 km with a position  
<sup>122</sup> uncertainty of 40 m. The beacon-to-glider performance, however, deteriorated due to missed  
<sup>123</sup> contacts outside the duct. In 2017, gliders were deployed in a region with no ice coverage.  
<sup>124</sup> Ranges were linearly scaled by a statistical description of sound speed observations taken  
<sup>125</sup> during the experiment,  $1450 \pm 6.5$  m/s (Graupe *et al.*, 2019). This resulted in an error  
<sup>126</sup> of 550 m, which was reduced by a factor between 4 and 5, depending on the dive, using a  
<sup>127</sup> post-processing acoustic arrival matching method. Both cases exploit the lower duct for high  
<sup>128</sup> fidelity communication at long ranges. Unintuitively, the smaller nature of our deployment

<sup>129</sup> during ICEX20 is not a simplifying factor. For source depths typical to vehicle operations,  
<sup>130</sup> 30 to 200 m, a shadow zone spans from 2 to 6 kilometers in range ([Schmidt and Schneider, 2016](#)).  
<sup>131</sup>

<sup>132</sup> Compared to the previous small scale navigation efforts, the approach in this paper  
<sup>133</sup> integrates real-time model-aided data processing to estimate a representative sound speed  
<sup>134</sup> along a path from source to receiver, leveraging climatology, *in situ* data, and fast acoustic  
<sup>135</sup> modeling. The paper is organized as follows. Section [II](#) details the experimental conditions  
<sup>136</sup> during ICEX20. Given that there is no GNSS ground truth for the vehicle position while  
<sup>137</sup> underway, we first evaluate the real-time ranging performance of GPS-linked beacon-to-  
<sup>138</sup> beacon communication events in section [III](#). Section [IV](#) uses insights from field data to  
<sup>139</sup> introduce a new ray filtering algorithm to improve range estimation. Section [V](#) emulates the  
<sup>140</sup> real-time processing pipeline to re-position beacon-to-beacon events and re-navigate AUV  
<sup>141</sup> *Macrura*.

<sup>142</sup> **II. OVERVIEW OF THE ICEX20 EXPERIMENT**

<sup>143</sup> The results from this paper derive from data taken while deploying the AUV *Macrura*, a  
<sup>144</sup> custom Bluefin-21, during the Ice Exercise 2020 (ICEX20), in the Beaufort Sea, from March  
<sup>145</sup> 8 to 11, in double-ducted and ice-covered conditions. The AUV deployment was supported  
<sup>146</sup> by the Integrated Communication and Navigation Network (ICNN) ([Randeni et al., 2020](#),  
<sup>147</sup> [2021](#); [Schneider et al., 2020](#)), a specialized implementation of the LBL solution. The ICNN  
<sup>148</sup> was initially developed via numerous virtual experiments to push the boundaries of algo-  
<sup>149</sup> rithms and interfaces between different hardware components. The simulation approach  
<sup>150</sup> serves as a testbed for robustness to produce better results than post-processing previous  
<sup>151</sup> field data. The simulation capabilities are largely physics-driven with a modular system of  
<sup>152</sup> systems approach—an environmental simulator with sub-components for the ocean, includ-  
<sup>153</sup> ing Arctic ice drift and ocean acoustic propagation; a vehicle simulator with sub-components  
<sup>154</sup> for vehicle dynamics and navigation; a topside hardware simulator and acoustic communica-  
<sup>155</sup> tions simulator, both with a software-only configuration and a hardware-in-the-loop version  
<sup>156</sup> ([Schneider and Schmidt, 2018](#)). The virtual environment similarly emulates the interfaces  
<sup>157</sup> between the real components to test the entire software pipeline. Both simulation capabili-  
<sup>158</sup> ties are integral to mission success.

<sup>159</sup> The ICNN is comprised of four ice buoys, in a loose rectangle, roughly 2 km away from a  
<sup>160</sup> central ice camp with a topside computer, as shown in Fig. 1. The AUV and each ice buoy are  
<sup>161</sup> outfitted with a WHOI Micro-Modem ([Singh et al., 2006](#)), with a four-element receiver array  
<sup>162</sup> and a single transmitter, one-tenth of a millisecond resolution. Acoustic messages were sent

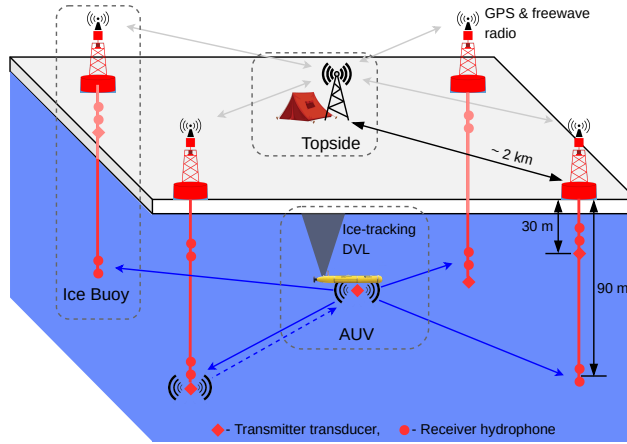


FIG. 1. A schematic overview of the Integrated Communication and Navigation Network (ICNN), which provides joint data-transfer and tracking between AUV and a human decision maker at Topside.

with a 10 kHz carrier frequency, 5 kHz bandwidth, and phase-shift keying (PSK) modulation on a thirty-second cycle, giving room for two-way communication throughout the mission volume. The receive and transmit elements were split between shallow and deeper depths (30 and 90 m, respectively) to provide better coverage across the shadow zone. While each buoy only has one transmit depth, all buoys have both receive depths but the active receive layer is consistent across all buoys. The design of the ICNN enables a self-adapting network to transmit and receive at the optimal depth to maintain contact with the AUV ([Schneider et al., 2020](#)). The buoys do not encompass the full horizontal range of the vehicle but are positioned to minimize overlap in trilateration for spherical positioning ([Deffenbaugh et al., 1996a](#)).

To balance competing uses of the acoustic channel, the network uses a single synchronized digital communication packet to provide both tracking and data to the operator.

175        1. The AUV, running an ice-tracking DVL and an onboard hydrodynamic model, broad-  
176        casts its perceived location on a scheduled, time-synchronized message via WHOI  
177        Micro-Modem

178        2. Four ice buoys, each outfitted with a WHOI Micro-Modem, receive messages from the  
179        AUV and send that information over freewave radio to a Topside computer

180        3. The topside computer converts travel times into range estimates using a stochastic  
181        embedded prediction of the horizontal group velocity via BELLHOP ray tracing code  
182        ([Porter, 2011](#)) coupled with an updatable Virtual Ocean ([Bhatt et al., 2021](#); [Schneider](#)  
183        and [Schmidt, 2018](#))

184        4. The topside computer calculates a new position by trilaterating the range estimates

185        5. The position differential, not the absolute position, is broadcast to the vehicle to  
186        update its navigation solution and be robust to latency and intermittency

187        In the face of GNSS-denied navigation, this approach was anecdotally successful, as shown

188        in 2. The AUV *Macrura* was deployed through a hydrohole from an ice camp but recovered  
189        through an emergency hydrohole. A random disk error stalled the AUV underneath the ice  
190        but did not prevent it from transmitting its location. Due to an incoming storm, a team  
191        placed a physical marker on the ice at the location. Three days later, *Macrura* was found

192        within a meter of the marker. We view the emergency recovery as qualitative proof of the  
193        robustness of this navigation approach. Nonetheless, this paper specifically addresses the  
194        third and fourth steps—the conversion of travel time into range and its effect on trilater-

195 ation. By focusing on range estimates between GPS-tracked beacons, and re-running the  
 196 trilateration pipeline, the results are decoupled from all other mechanisms in the ICNN.

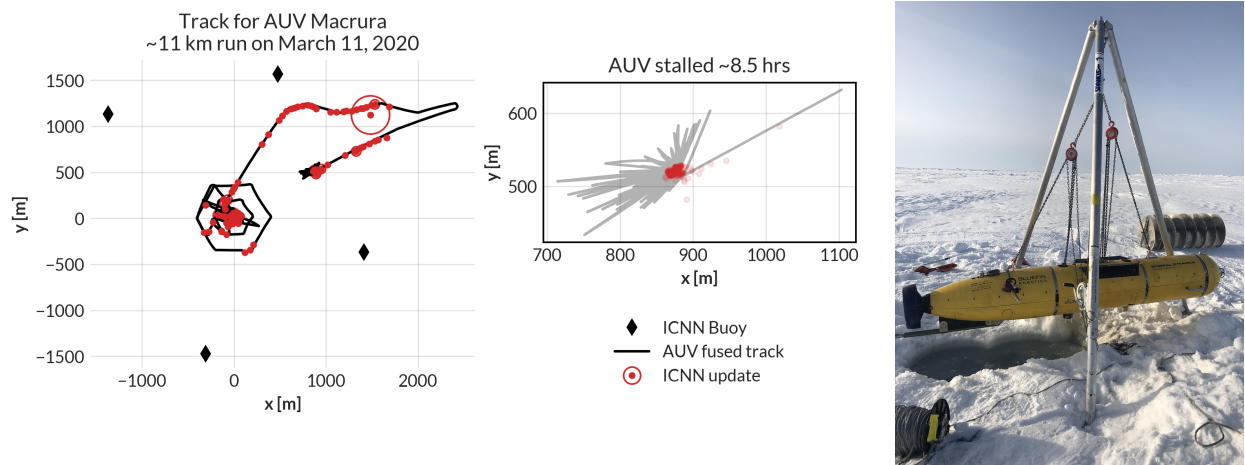


FIG. 2. The under-ice mission track for AUV Macrura, including the position updates as it stalled underneath the ice overnight. A marker was placed on the ice at the vehicle’s estimated self-location. It was recovered after a three day storm within a meter of the marker.

197 An important component to our navigation solution is an accurate estimation of the sound  
 198 speed profile. Previous field experience, during the Ice Exercise 2016 (ICEX16), demon-  
 199 strated the negative effects of the Beaufort Lens on tracking and communication ([Schmidt](#)  
 200 [and Schneider, 2016](#)). Fig. 3 shows historical, modeled, and *in situ* data for both ICEX16  
 201 and ICEX20. These three input streams were selected to mirror the information available  
 202 on a submarine (personal conversation with LT B. Howard and LT CDR D. Goodwin).  
 203 The SSP information was compressed with a basis representation and sent via lightweight  
 204 digital acoustic message to the AUV ([Bhatt et al., 2021](#)). All modeled data comes from  
 205 HYCOM ([Chassagnet et al., 2007](#)), which does not seem to capture the forcing mechanisms  
 206 that cause the Beaufort Lens. For ICEX16, the data-driven profile was sourced from nearby

207 Ice Tethered Profilers (ITP) after the field experiment (Krishfield *et al.*, 2008; Toole *et al.*,  
208 2011) and exhibits a fairly low lens; the historical profile is from the World Ocean Atlas.  
209 For ICEX20, the chosen weights (data-driven) profile derives from a basis representation  
210 estimation of initial CTD casts taken on site, showing an intense warm water intrusion; the  
211 baseline (historical) profile, showing moderate ducted conditions, comes from the average  
212 of March 2013 data. This month best matched sea ice and sound speed conditions at the  
213 beginning of ICEX20 (Bhatt *et al.*, 2021). It is important to note that all profiles that do  
214 show the Beaufort Lens do so with different local sound speed maxima at different depths,  
215 reflective of the wide range of lens properties observed for all ITP data in the region. The  
216 variability of the lens height and prominence is the main reason an updatable SSP was  
217 integrated into the ICNN solution.

218 During ICEX20, the HYCOM profile was available but never deployed. For post-  
219 processing comparison, we introduce both the HYCOM profile and an isovelocity case,  
220  $1441.8 \pm 3.7$  m/s, as the mean and standard deviation of the observed sound speed profile  
221 over the first 200 m.

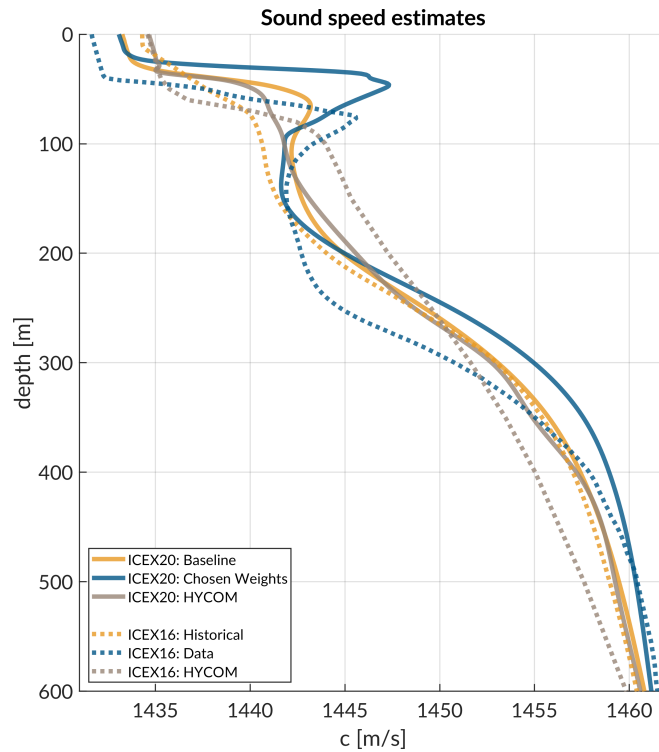


FIG. 3. Sound speed conditions for historical (baseline), data (chosen weights), and HYCOM model for both ICEX16 and ICEX20.

222 **III. REAL-TIME PSEUDORANGE ANALYSIS**

223 Because the vehicle's navigation solution during a mission can only be evaluated on the  
224 basis of the error estimates sent, a sister experiment for validating the real-time ranging  
225 approach was implemented. Ice buoy modems were run as "virtual vehicles" at a fixed  
226 depth, receiving position updates from the other beacons as well as a camp site modem  
227 lowered to 20 m. Figure 4 shows successful events sorted by source depth. In this analysis,  
228 we assume there is insignificant displacement between the GNSS puck surface expression and  
229 subsurface modem; this is supported by unusually low observed ice drift rates, on average,  
230 just 0.7 cm/s.

231 **A. Minimal bounce criteria (MBC)**

232 The fundamental challenge to implement GNSS-like navigation, especially in an acousti-  
233 cally complex propagation environment, is characterizing a single sound speed to compensate  
234 for the effects of ray refraction and reflection. The use of the acoustic modem network for  
235 tracking relies on the accurate estimates of travel times between the submerged platform  
236 and LBL beacons, supported by clock synchronization and a pre-determined scheduling of  
237 acoustic events. For the Beaufort Lens in particular, the strong multipath effects make it  
238 virtually impossible to deterministically predict the modem's detected arrival time.

239 Instead, for each individual modem  $i$ , an embedded stochastic tracking framework is used  
240 to provide a running estimate of the horizontal group velocity  $u_{i,j}$  for the conversion from  
241 travel time to range from modem  $j$ , with the ultimate goal of matching the naive group

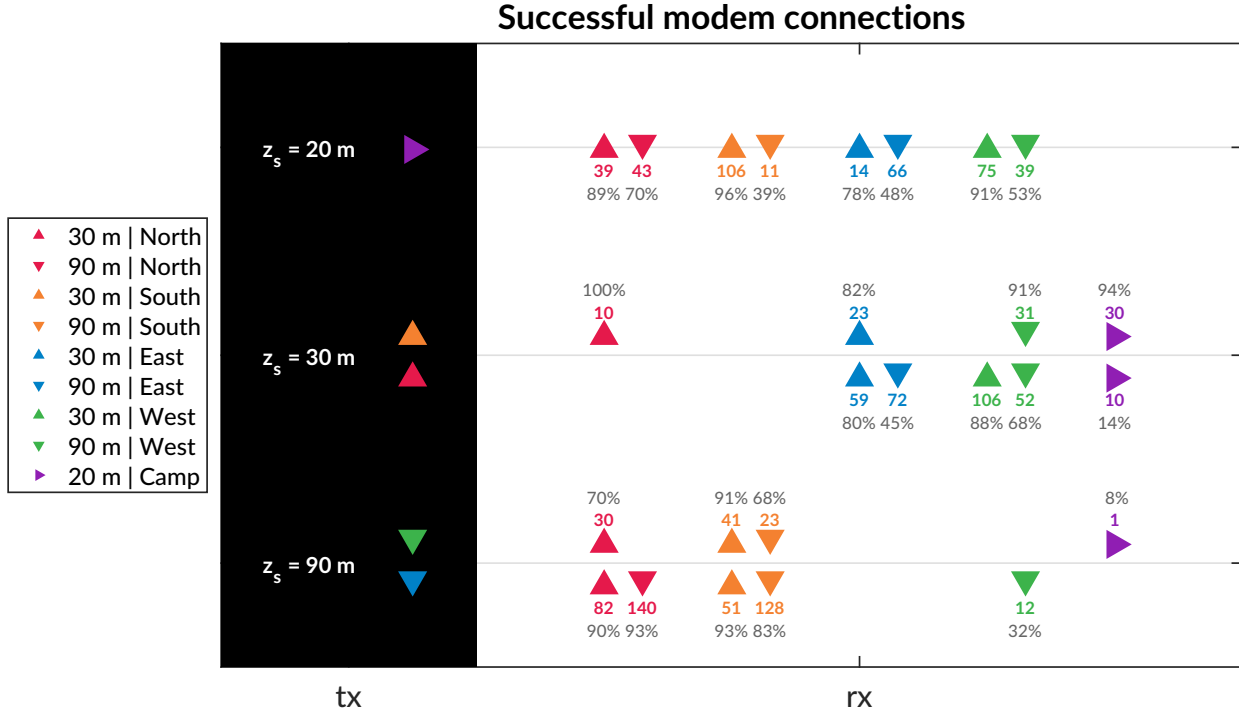


FIG. 4. An overview of the modem experiment by source and receiver depth and position with the number of successful decodings and the percent success rate, defined as the ratio of decoded to detected. The black column on the left, *tx*, shows the source depth,  $z_s$ . The column on the right, *rx*, shows the receivers with the amount of good contacts. The orientation of the triangles—sideways, upwards, and downwards—corresponds to depths of 20, 30, and 90 m.

<sup>242</sup> velocity, i.e. the GPS-recorded distance between two nodes divided by the modem-recorded  
<sup>243</sup> one way travel time between them.

<sup>244</sup> In the ICEX20 configuration, the acoustic tracking is running on the topside computer,  
<sup>245</sup> which controls the ICNN. Here we assume that the group velocities  $u_{i,j}$  are smoothly varying  
<sup>246</sup> over the course of a vehicle mission, i.e., with respect to range, mission time, and the

<sup>247</sup> frequency of updates relative to vehicle motion. The group velocity is tracked on a thirty-  
<sup>248</sup> second cycle using predictions from the *Virtual Ocean* infrastructure.

<sup>249</sup> When the topside tracking framework receives a modem message, with a time delay,  $\Delta t$ ,  
<sup>250</sup> from one of the range modems, it will request a new estimate of the group velocity and its  
<sup>251</sup> associated uncertainty. The group velocity estimate is found using the vehicle's reported  
<sup>252</sup> depth and the extrapolated navigation solution for range,  $\hat{r}$ , as inputs for the ray tracing  
<sup>253</sup> program. The latter returns an impulse response estimate in the form of ray travel times  
<sup>254</sup>  $dt_j$  and amplitudes  $a_j$  for that range and depth.

<sup>255</sup> The initial call to BELLHOP is over a local grid centered at the range and depth posited  
<sup>256</sup> by the onboard tracking solution. Compared to a point solver, solving for arrivals on a grid  
<sup>257</sup> minimizes the impact of numerical resolution in the propagation model. The resulting ray  
<sup>258</sup> traces may represent paths that would reach a receiver in a real application but might not  
<sup>259</sup> be recognized by the numerical solver as a viable detection. The grid is initialized as  $11 \times 11$   
<sup>260</sup> points spanning 10 m horizontally and 20 m vertically. The horizontal dimension reflects the  
<sup>261</sup> accumulated position error given a thirty-second communication cycle; the vertical dimen-  
<sup>262</sup> sion reflects how, computationally, eigenrays of the same timefront seem to stack vertically  
<sup>263</sup> in the water column. For each grid point, BELLHOP produces a number of arrivals resulting  
<sup>264</sup> from multiple propagation paths for any source-receiver pair. Using only the  $N_0$  rays with  
<sup>265</sup> neither surface nor bottom bounces, it will then estimate the current group velocity  $u$  from  
<sup>266</sup> a power weighted average of the ray travel times,

$$u = \frac{\hat{r} \sum_{n=1}^{N_0} a_n^2}{\sum_{n=1}^{N_0} dt_n a_n^2}, \quad (1)$$

<sup>267</sup> and the associated weighted standard deviation,

$$\sigma_u \simeq \sqrt{\frac{\sum_{n=1}^{N_0} (dt_n - \hat{r}/u)^2 a_n^2}{\sum_{n=1}^{N_0} a_n^2}} \frac{u^2}{\hat{r}} \quad (2)$$

<sup>268</sup> If no direct paths exist, i.e.  $N_0 = 0$ , then the group velocity is computed using the same

<sup>269</sup> algorithm for the ray arrivals with one bounce, and so on.

<sup>270</sup> Finally, the pseudorange is calculated simply as

$$r_{i,j} = u_{i,j} \Delta t_{i,j} \quad (3)$$

<sup>271</sup> Thus the NBC method assumes the signal detected by the modem will be dominated

<sup>272</sup> set of paths with the least number of boundary interactions. Importantly, this stochastic,

<sup>273</sup> ensemble method for group velocity calculation can run in real-time, appearing to be orders

<sup>274</sup> of magnitude faster than other post-processing methods which seek to determine the specific

<sup>275</sup> ray itself that best matches a prominent indicator from the arrival structure. The BELLHOP

<sup>276</sup> simulation that runs this calculation uses 3600 rays with launch angle fan of -60 to 60 degrees,

<sup>277</sup> a representative depth dependent sound speed profile, and a range dependent bathymetry.

<sup>278</sup> **B. Pseudorange error metrics**

<sup>279</sup> The sister modem experiment generated 811 beacon to beacon communication events with

<sup>280</sup> their own real-time MBC group velocity predictions. Given the complexity of the ICNN

<sup>281</sup> system, this experiment did not collect an exhaustive set of data across all buoy, source

<sup>282</sup> depth, receive depth, and sound speed combinations. The algorithm generally overestimates

<sup>283</sup> pseudoranges because it resolves the effective sound speed for the most direct path.

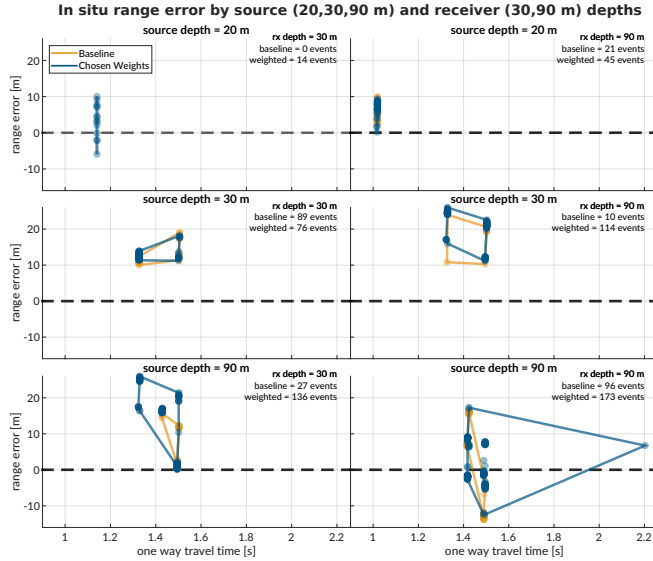


FIG. 5. The real-time range error by source (20, 30, and 90 m) and receiver (30 and 90 m) pairings for both sound speed estimates used during ICEX20. The amount of communication events is notated in the top right of each panel. The dashed line indicates no range error, and the boundary drawn indicates scope of the range error as a function of one way travel time.

284 Figure 5 shows the range error boundary for both SSP inputs used in ICEX20. A promising sign that the MBC method adapts sound speed realistically is no obvious error growth  
 285 as travel time increases. The baseline SSP ( $n=243$  events) has an absolute pseudorange  
 286 error of  $11.38 \pm 4.23$  m; the weighted SSP ( $n=568$ ),  $11.36 \pm 8.12$  m. The discrepancy  
 287 between these two is largely due to outlier events only contained in the weighted SSP set.  
 288 Where there is overlap between sound speed conditions used for the real-time MBC, the  
 289 pseudorange error difference is no more than a few meters. The overarching results show  
 290 that sound speed estimates derived from eigenrays for a local grid, as opposed to a singular  
 291 point, are accurate enough to support vehicle navigation. While the NBC looks for just the  
 292 least complex multipath, the high density of launch angles almost always guarantees a direct  
 293 least complex multipath, the high density of launch angles almost always guarantees a direct

<sup>294</sup> path. Nonetheless, the consistent overestimation of pseudorange invites further analysis into  
<sup>295</sup> acoustic arrival matching.

<sup>296</sup> **C. Eigenray identification for beacon-to-beacon events**

<sup>297</sup> Figs. ?? each show eigenrays for three sound speed environments for source depths of 20,  
<sup>298</sup> 30, and 90 m, respectively. It is important to note that BELLHOP produces an abundance  
<sup>299</sup> of eigenrays; the ones displayed here are chosen by travel time proximity to the recorded  
<sup>300</sup> data. With this filter, the chosen eigenrays show a greater amount of surface interactions as  
<sup>301</sup> the SSP duct conditions increase.

<sup>302</sup> This is likely driven by the prominence of the duct.

<sup>303</sup> The ultimate goal of the MBC and NBC algorithms is to provide a reliable, physically  
<sup>304</sup> intuitive interpretation of the acoustic propagation models, without taking on the added  
<sup>305</sup> burden of regularly identifying specific paths that may connect any given source-receiver  
<sup>306</sup> pair in the network. As shown, the quadruple surface bounce prediction produced by the  
<sup>307</sup> power-weighted NBC for the North-South link is consistent with the time filtered eigenray.

<sup>308</sup> The figures do not show bottom bounce paths due to the steeper angles at which they travel;  
<sup>309</sup> however, these paths do appear in the simulations as well. For the North-South link, with  
<sup>310</sup> the source at 30 m depth, the simulations include rays with a single bottom bounce which  
<sup>311</sup> would match the predicted travel time of 4.181 seconds. With the source at 90 meters, as is  
<sup>312</sup> the case for the East-West link, rays with surface-bottom and bottom-surface bounces (for  
<sup>313</sup> 2 bounces total) are also present.

314

### 1. Source depth of 20 m

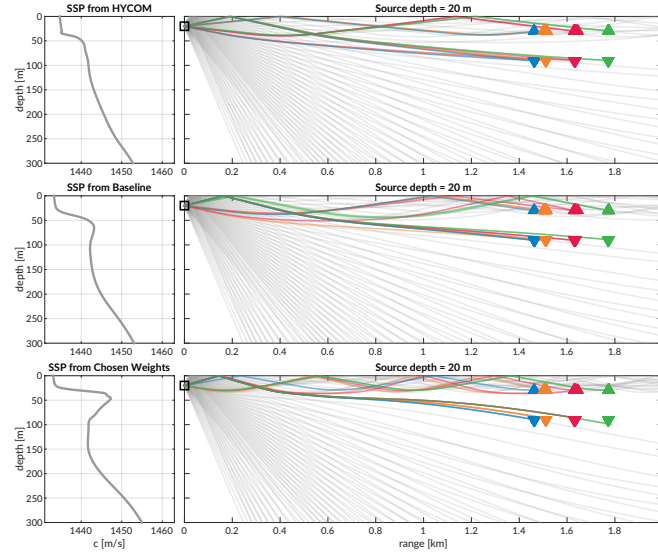


FIG. 6. Eigenrays for beacon to beacon events for each sound speed with a nominal source depth of 20 m. The beacons are highlighted in color/marker coding in Fig. 4. The eigenrays are curated from BELLHOP by travel time proximity and are traced in the representative receiver colors over a total ray fan in gray.

315

### 2. Source depth of 30 m

316

### 3. Source depth of 90 m

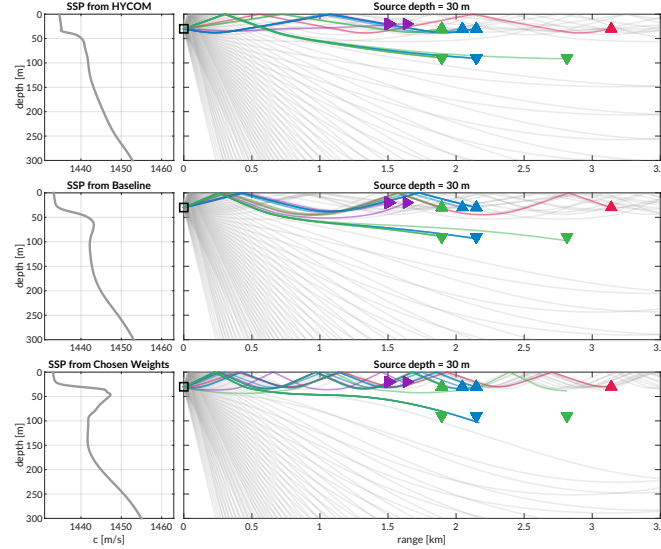


FIG. 7. Eigenrays for beacon to beacon events for each sound speed with a nominal source depth of 30 m. The beacons are highlighted in color/marker coding in Fig. 4. The eigenrays are curated from BELLHOP by travel time proximity and are traced in the representative receiver colors over a total ray fan in gray.

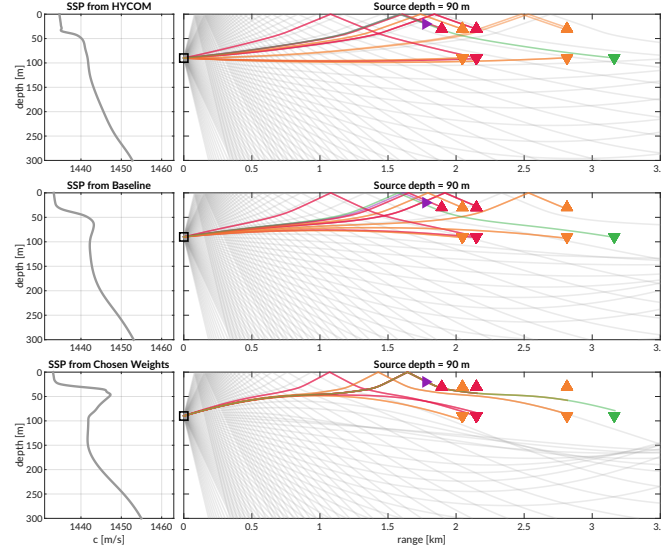


FIG. 8. Eigenrays for beacon to beacon events for each sound speed with a nominal source depth of 90 m. The beacons are highlighted in color/marker coding in Fig. 4. The eigenrays are curated from BELLHOP by travel time proximity and are traced in the representative receiver colors over a total ray fan in gray.

<sup>317</sup> **IV. POST-PROCESSED PSEUDORANGE ANALYSIS**

<sup>318</sup> From all events recorded during the modem test experiment, there are 1242 successfully  
<sup>319</sup> decoded beacon-to-beacon events. Only these events are used to evaluate ranging accuracy,  
<sup>320</sup> as the ICNN was not configured to use receptions with failure flags. Thus, a post-processing  
<sup>321</sup> analysis that emulates the real-time navigation engine was run to overcome the unequal  
<sup>322</sup> distribution of communication events with respect to depth, range, and sound speed status.

<sup>323</sup> It is important to note that the value for the extrapolated range,  $\hat{r}$ , is only tracked when  
<sup>324</sup> the modem runs the vehicle behavior; thus we replace  $\hat{r}$  with the GPS-tracked range for all  
<sup>325</sup> modem events. Because  $\hat{r}$  converges to the correct solution, a comparison of  $\hat{r}$  with the GPS-  
<sup>326</sup> tracked range shows a normal, zero-centered distribution within the bounds of GPS drift.

<sup>327</sup> The present analysis therefore seeds realistic but “omniscient” knowledge of the extrapolated  
<sup>328</sup> range and leverages the post-processing pipeline to more thoroughly evaluate the acoustic  
<sup>329</sup> range estimate for all modem events, with three relevant sound speed sources, and both  
<sup>330</sup> group velocity criterion. Accordingly, the results in this section evaluate the utility of the  
<sup>331</sup> algorithms and sound speed sources, divorced from their role in the ICNN while maintaining  
<sup>332</sup> real-time relevance.

<sup>333</sup> **A. Nearest bounce criteria (NBC)**

<sup>334</sup> As shown in the eigenray traces of Fig. 7, the extent of ray bending and repeated  
<sup>335</sup> reflections is extremely dependent on the sound speed profile. An isovelocitity approach  
<sup>336</sup> would completely miss this nuance; our field-tested approach that only resolved the simplest

path is unlikely to resolve the one that triggers modem detection. Based on this insight, a new algorithm, the nearest bounce criteria (NBC), is a slight modification from the MBC and includes multipath as a new dimension of information to exploit. This metric, while run in post-processing, adds a negligible amount of computation for real-time efficacy.

Given a running estimate for the horizontal group velocity  $u_{i,j}$  between nodes  $i$  and  $j$ , the navigation system has an extrapolated value for range,  $\hat{r}$ , and a recorded travel time,  $\Delta t_{i,j}$ . Instead of using only the  $N_0$  rays with neither surface nor bottom bounces to estimate group velocity and subsequently moving to incremental number of bounces only when no valid direct path solutions exist, we solve for the power weighted average of the ray travel time for the  $N_k$  rays with  $k$  bounces,

$$t_k = \frac{\sum_{n=1}^{N_k} dt_n a_n^2}{\sum_{n=1}^{N_k} a_n^2}, \quad (4)$$

find the nearest matching power weighted average to recorded travel time,

$$t_{i,j,k} = \min_{k=0,1,2,\dots} |t_k - \Delta t_{i,j}| \quad (5)$$

predict a group velocity,

$$u_{i,j} = \frac{\hat{r}}{t_{i,j,k}} \quad (6)$$

and estimate the range as was done previously.

$$r_{i,j} = u_{i,j} \Delta t_{i,j} \quad (7)$$

This method selects a different group velocity based on the multipath arrival structure, as the detected arrival is not always the first arrival or the direct path and could even be masked by noise or blocked temporarily (Deffenbaugh *et al.*, 1996b). We manually cap the

353 number of bounces to 4 because of the smaller operational scale and the attenuation accrued  
 354 with many surface interactions. Bottom bounces are not encoded separately because of ray's  
 355 tendency to refract upward, not due to information limitations.

356     **B. Effective sound speed predictions**

357     The minimal and nearest bounce algorithms are applied with the three sound speed inputs  
 358 shown in Fig. 7. The resulting predicted group velocities for all source depths are shown in  
 359 Fig 9.

360     The goal of the group velocity estimation is to converge towards the implied sound speed,  
 361 i.e. the GNSS-derived range divided by the recorded travel time. For a 30 m receiver depth,  
 362 the NBC shows more overlap with data-derived values as it classifies multipath more cor-  
 363 rectly. For a 90 m receiver depth, the overlap is less accurate due to computational con-  
 364 straints of a limited fan of rays entering the shadow zone rendering a less reliable simulated  
 365 times of arrival packet.

366     As the environmental and ray filtering method become better representations of the real  
 367 ocean, the lower the expected mismatch is between the implied and estimated effective  
 368 sound speeds. Analysis shows that the higher multipath classification produces more ac-  
 369 curate sound speed predictions, likely driven by a tighter and/or sparser bundle of rays.  
 370 However, that data are too small to draw significant conclusions. Discontinuities in mul-  
 371 tipath classification verify our hypothesis for its importance to a smoothly varying group  
 372 velocity, as shown in the cluster for a receiver depth of 30 m, where HYCOM jumps from

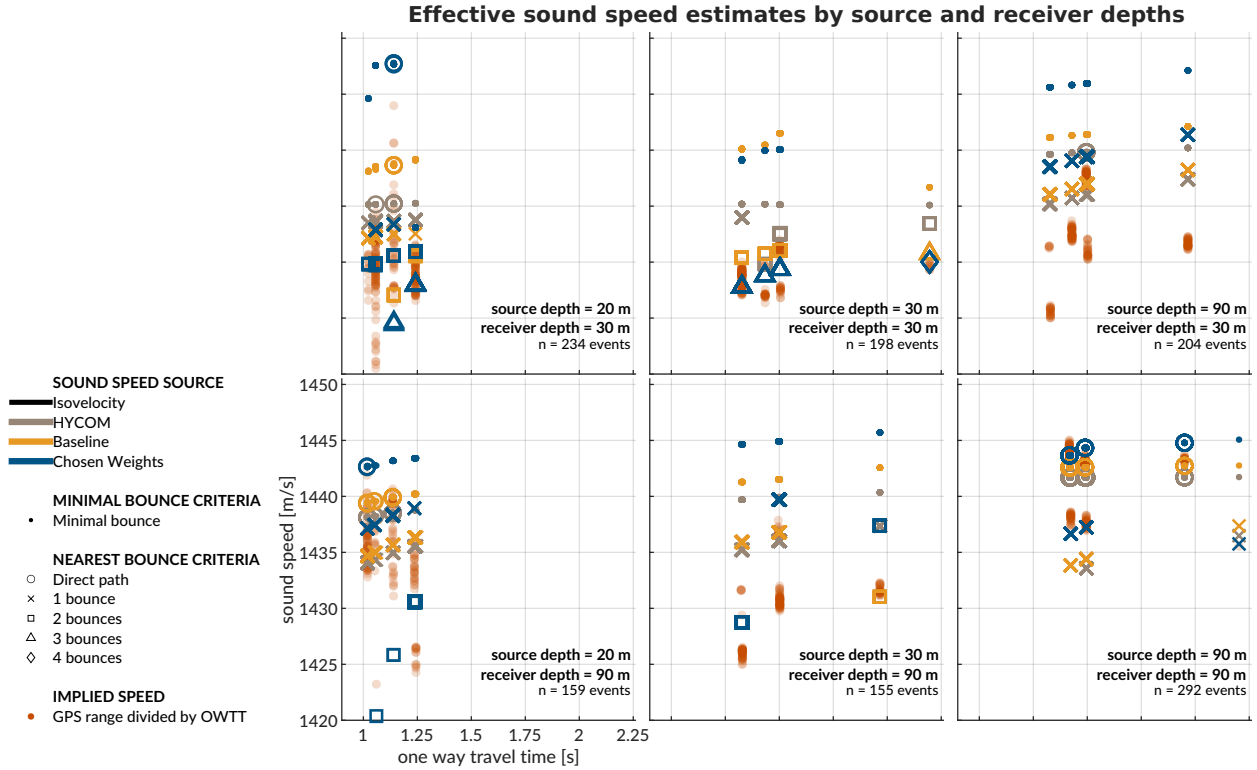


FIG. 9. A comparison of group velocity predictions for all beacon to beacon events in post-processing with a source depth of 30 m, with group velocity on the y-axis and recorded travel time on the x-axis. The left panel is for a receiver depth of 30 m; the right panel for 90 m. The sound speed source is indicated by color. The minimal and nearest bounce criterion are distinguished by different marker shapes, compared to the separately colored red dots showing the naive, data-driven group velocity calculation.

373 one to two bounces amidst the baseline SSP and weighted SSP smoothly increasing while  
 374 consistently seeing two and three bounces, respectively.

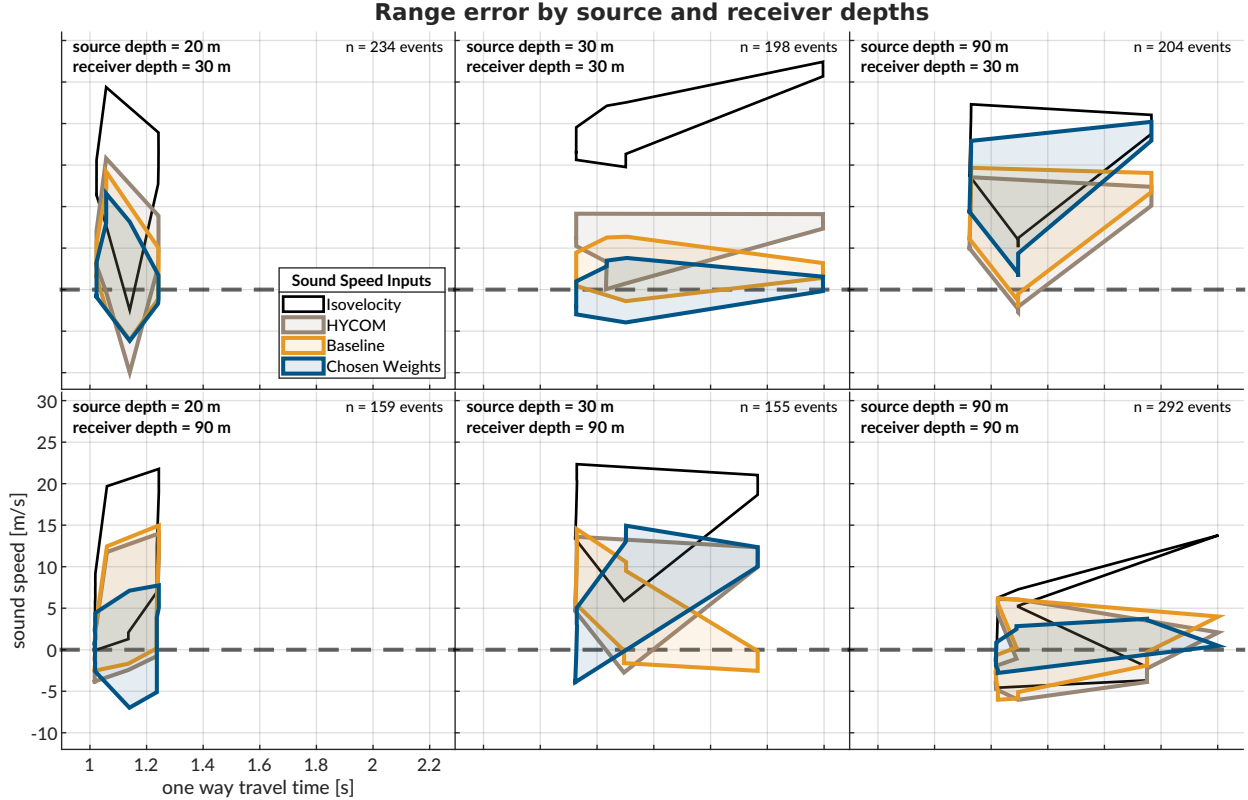


FIG. 10. The post-processed range error for source depths of 20, 30, and 90 m, and receiver depths of 30 and 90 m. The dashed gray line shows no error. The shaded region connects the range performance across all events.

375      **C. Pseudorange error metrics**

376      Fig. 10 shows the directional range error footprints for all three sound speed inputs with  
 377      respect to OWTT, separated by source and receiver depth configurations. The weighted  
 378      SSP range error generally has the smallest and most zero-centered footprint. The one case  
 379      it does not is for the source-receiver pairings between 30 and 90 m in depth. The increased  
 380      error for these reciprocal transmission paths is most likely driven by the computational  
 381      artifacts encountered when propagating through the steep sound speed gradients of the lens

<sup>382</sup> and through the shadow zone. All other source depth pairings are significantly improved  
<sup>383</sup> using the chosen weights compared to HYCOM or the baseline.

<sup>384</sup> When using a linear scaling to convert travel time into range, any offset between the  
<sup>385</sup> assumed sound speed and the horizontal group velocity produces unconstrained error with  
<sup>386</sup> increasing receiver distance. Most importantly, we see the consequences of the adaptive  
<sup>387</sup> group velocity in that range error does not strictly increase with OWTT.

<sup>388</sup> The improvement from MBC to NBC is most evident for the realistic sound speed; while  
<sup>389</sup> the HYCOM SSP improves from a median absolute range error of 6.41 to 4.61 m, the  
<sup>390</sup> baseline SSP improves from 10.30 to 2.27 m, and the weighted SSP improves from 13.28  
<sup>391</sup> to 2.12 m. Table I shows further statistics on the absolute range error by SSP and group  
<sup>392</sup> velocity algorithm. The order of magnitude improvement in the ducted SSPs demonstrate  
<sup>393</sup> the effectiveness of the algorithm exploiting the multipath conditions.

<sup>394</sup> As shown in table I, there is a striking maximum range error of 1491 m for the weighted  
<sup>395</sup> SSP in the minimal bounce criteria. There are 10 events from South transmitting at 30 m  
<sup>396</sup> depth to North receiving at 30 m depth. The OWTT spread is from 2.1958 to 2.1963 s; the  
<sup>397</sup> naive group velocity is 1429.3 to 1430.1 m/s; and the GPS-tracked range is from 3138.54 m  
<sup>398</sup> to 3140.87 m. This example ends up being an excellent case study for how sound speed and  
<sup>399</sup> multipath fidelity work in concert to minimize range error. The large error in this instance  
<sup>400</sup> is driven by the MBC unexpectedly defaulting to a bottom bounce with a much greater  
<sup>401</sup> OWTT. The NBC classifies the multipath as 4 bounces, reducing the range error from  
<sup>402</sup> greater than a kilometer to less than a meter. While there is no actual way of knowing if  
<sup>403</sup> this is the correct multipath structure, the range error is remarkably small, at 0.025%. This

|             | Baseline |       | Chosen Weights |       | HYCOM |       |
|-------------|----------|-------|----------------|-------|-------|-------|
|             | MBC      | NBC   | MBC            | NBC   | MBC   | NBC   |
| minimum [m] | 0.01     | 0.00  | 0.00           | 0.00  | 0.11  | 0.01  |
| 25th % [m]  | 4.96     | 0.99  | 6.26           | 0.95  | 3.30  | 2.25  |
| median [m]  | 10.30    | 2.27  | 13.28          | 2.12  | 6.41  | 4.61  |
| 75th % [m]  | 15.81    | 5.51  | 19.75          | 4.11  | 10.92 | 7.46  |
| maximum [m] | 22.52    | 14.96 | 1491           | 20.21 | 19.55 | 15.81 |

TABLE I. A comparison of range estimation metrics for each sound speed source and group velocity estimation algorithm for all 1283 beacon to beacon events via post-processing. The 0th (minimum), 25th, 50th (median), 75th, and 100th (maximum) percentiles are shown to the range resolution afforded by the WHOI Micro-Modem. There are a few outliers that drive the mean to be higher than the median.

404 pattern of not choosing the minimal observed bounce structure is consistent across all SSPs;  
 405 the baseline goes from 1 to 3 bounces and HYCOM goes from 0 to 2 bounces. Notably,  
 406 the baseline and HYCOM range errors are never egregiously large, but are nonetheless  
 407 improved with the NBC algorithm. Thus, for acoustically complex environments, the NBC  
 408 has a disproportionately positive impact as the estimated SSP approaches the desired SSP.

<sup>409</sup> **V. TRILATERATION FOR ICEX20 FIELD DATA**

<sup>410</sup> To overcome potentially intermittent acoustic communication, the operational paradigm  
<sup>411</sup> of the ICNN computes corrections relative to the trilaterated position estimates transmitted  
<sup>412</sup> by the vehicle, rather than transmitting the updated positions themselves. The reliability  
<sup>413</sup> of the correction is directly linked to how accurately the travel time measurements are  
<sup>414</sup> converted to pseudoranges. This section aims to resolve that tension by reevaluating the  
<sup>415</sup> trilateration results with respect to the MBC and NBC algorithms. The MBC/NBC sound  
<sup>416</sup> speed estimates were tracked independently for each transmitter-receiver pair; although the  
<sup>417</sup> sound speed was expected to be locally smooth near a given receiver, no such assumption  
<sup>418</sup> was enforced between distinct acoustic links.

<sup>419</sup> **A. Re-positioning beacon to beacon events**

<sup>420</sup> When the beacons ran as virtual vehicles, the ICNN did not have access to that buoy's  
<sup>421</sup> GPS data stream except for what was sent via digital acoustic message. The static nature of  
<sup>422</sup> the experiment means that the initial estimate transmitted to the ICNN was in fact a ground  
<sup>423</sup> truth position. Therefore, a distribution of corrections from the ICNN, as shown in Fig. 11,  
<sup>424</sup> reflects positioning accuracy. The NBC clearly outperforms the MBC, with almost 80% of  
<sup>425</sup> the corrections below 6 meters and the median within the deployed GNSS puck precision  
<sup>426</sup> of 3 meters. By contrast, the MBC shows roughly 20% within the GNSS puck precision,  
<sup>427</sup> and separate peaks from 9–12 meters and 21–27 meters. This trimodal nature reflects the  
<sup>428</sup> distribution of reflections on the ice surface.

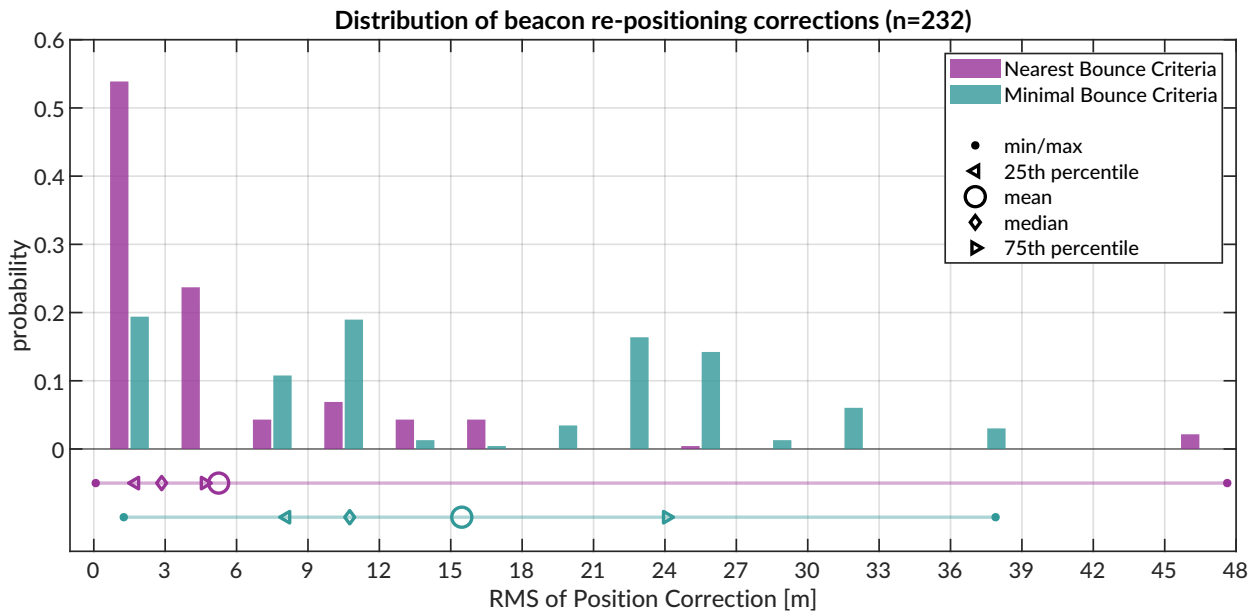


FIG. 11. Trilateration events; however, 264 entries are 2-beacon solutions, 22 are 3-beacon, and 2 are 4-beacon. When limited to only two ranging circles, the trilateration chooses the closer of the two intersection points. The x-axis is cut off at the upper limit for the NBC algorithm.

429 In several events, the MBC is unable to accurately estimate the effective sound speed for  
 430 one of the acoustic links, leading to a large positioning error. The NBC, however, better  
 431 resolves an approximation of the acoustic path. For example, in some trilateration solutions  
 432 for the Eastern buoy, the MBC shows a correction of more than a kilometer; the NBC is  
 433 two order of magnitudes less.

434 **B. Re-navigating AUV Macrura**

435 Up to this point, pseudorange estimation and localization have been evaluated on GPS-  
 436 linked beacon-to-beacon connections to validate the NBC algorithm. This analysis ports the  
 437 MBC and NBC algorithms to re-navigate the AUV *Macrura*.

438        The AUV dataset clearly exhibits instances where a receiver detects the same transmission  
 439      more than once. This is not surprising considering the complex multipath provided by  
 440      the Beaufort Lens. The 11 hour vehicle mission contains 3260 transmissions, 12938 total  
 441      detections, and 4704 successful receptions. Allowing receptions with PSK errors would  
 442      almost double the number of recorded multipath arrivals exploited for positioning, if a real-  
 443      time solution could correctly parse paths from different arrivals in the same thirty-second  
 444      cycle. Thus it remains a future endeavor to explore how failure mode information from  
 445      acoustic modems could be used to identify unsuccessful but otherwise trustworthy arrivals  
 446      to augment trilateration samples.

447        The following performance analysis is constrained to what the vehicle acted on in real-  
 448      time. AUV *Macrura* and the ICNN ran an adaptive depth behavior to maintain acoustic  
 449      communication on the insight that cross-layer links were more likely to fail than same-layer  
 450      ones. Accordingly, the vehicle dove deeper than 50 meters about 20% of the time it was  
 451      underway.

452        In contrast to the modem tests, where position correction illustrated re-positioning ac-  
 453      curacy, the re-navigation corrections are less valuable in the absence of GNSS ground truth.  
 454       The correction magnitude necessarily depends on the vehicle's internal navigation estimate,  
 455      which is prone to larger errors from sensor drifts, ocean currents, and other error not cap-  
 456      tured in the hydrodynamic model. Thus, larger corrections are not necessarily indicative of  
 457      worse performance. Navigation accuracy may be better described by trilateration error, the  
 458      RMS of the remaining pseudorange errors from each acoustic link.

459 Fig. 12 shows the correction magnitudes and trilateration errors for events with three or  
 460 more receptions during AUV operations. Whereas the MBC has a fairly bimodal nature,  
 461 with peaks centered around 10–15 and 35–40 m, the NBC favors smaller corrections, from  
 462 5–20 m, and has a long tail. The distribution of corrections are much larger than the  
 463 distribution of RMS error. It is apparent that, while both methods are quite successful,  
 464 there is strong evidence that the NBC achieves single meter accuracy.

465 **C. Investigating potential GNSS noise**

466 The fact that the bulk of the best performing re-navigation error exists within the pre-  
 467 cision of the GNSS unit deployed invites a further look into GNSS noise. In the Arctic,  
 468 GNSS performance worsens due to poor constellation coverage, larger ionospheric effects,  
 469 and multipath interference. The National Security Implications of Climate Change for U.S.  
 470 Naval Forces (Council, 2011) details some of the limitations of the Global Positioning Sys-  
 471 tem (GPS) at polar latitudes. Radio infrastructure that provides position corrections and  
 472 references does not regularly extend to polar regions. The effect is minor for surface platform  
 473 navigation —roughly 15 m of horizontal precision has been displayed at the North Pole—but  
 474 is significant enough to register against the modem’s detected travel times. Figure 13 zooms  
 475 in on the GNSS and OWTT noise relative to the ice movement for two pairs of modem buoy  
 476 connections. The two panels indicate the GPS drift as  $\delta R = \sqrt{\delta x^2 + \delta y^2}$  and temporal drift,  
 477  $\delta t$ , relative to the median OWTT recorded between the two modems. The dashed line is  
 478 scaled by a group velocity of 1440 m/s, such that if there were ideal sensor measurements  
 479 with no drift, all events should exist on or near the line.

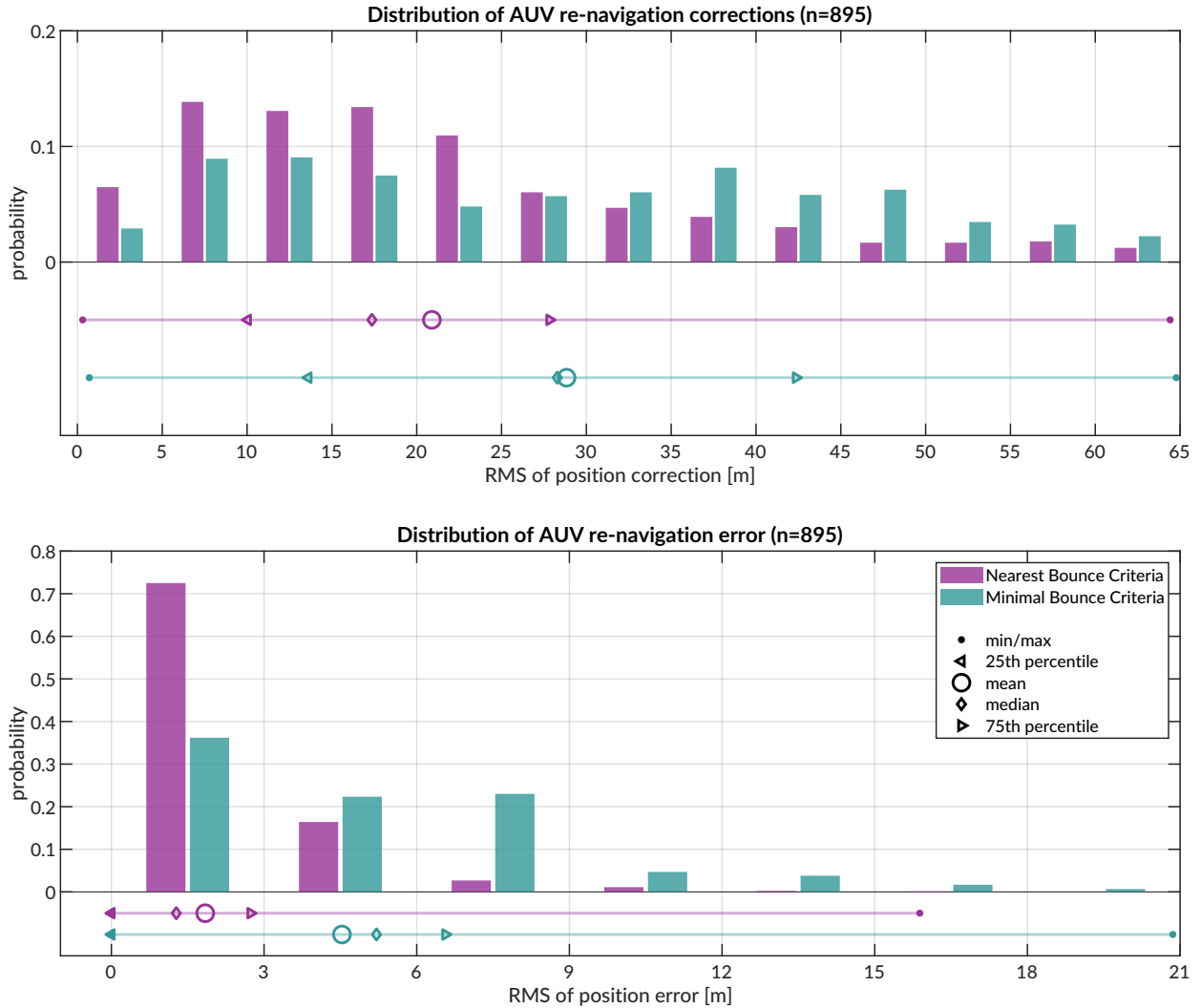


FIG. 12. Distribution of vehicle re-navigation corrections (top) and error (bottom) computed in post-processing for the Minimum and Nearest Bounce Criterion.

480 The top panel shows the connections between the North and East buoys. There is relative, i.e. non-rigid, ice movement between the North and East buoys, evidenced by events spanning the dashed line. But the height of the scatter plot is indicative of the precision of the GPS signal, as it remains consistent across many arrival time bands. Naturally, some minor offsets between these vertical bands relate to different operational configurations of

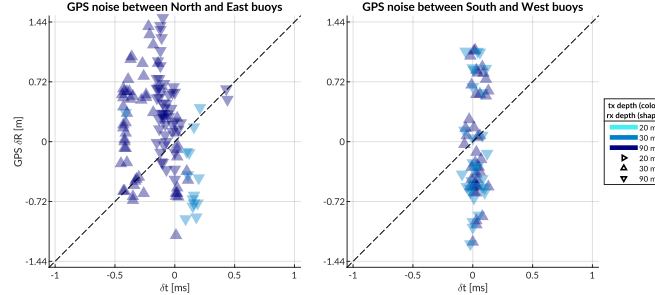


FIG. 13. A comparison of GPS drift (y-axis) versus OWTT drift (x-axis), colored by source and receiver depth. The physical link between North and East are shown on the top; South and West is on the bottom.

485 source and receiver depth. However, the large majority of events show vertical banding for  
 486 the same nominal  $\delta t$ , indicating the amount of GPS drift.

487 This idea of GPS drift relative to the same OWTT measurements is further indicated by  
 488 events between the other two buoys, South and West, in the bottom panel. These buoys are  
 489 moving in a more rigid ice floe and there is minimal impact by source and receiver depth  
 490 on the spread of OWTT. The GPS drift is much larger relative to the OWTT drift, which  
 491 is sensitive to acoustic scattering, multipath, and/or environmental microstructure.

492 These are just two subsets of the physical links that cover all four GPS modem buoys. The  
 493 GPS at camp is the least accurate due to the human activity and infrastructure occluding  
 494 the physical puck.

## 495 VI. DISCUSSION

496 Given the computational constraints of real-time modeling, the gridded approach facil-  
 497 itates enough multipath classification to build in a “ray ensemble” of characteristic group

498 velocities. This result is not always possible when aiming to find eigenrays to just an individual point, even with a higher density of launch angles. An important takeaway for those  
 499 interested in ray-based localization is leveraging a local grid to give BELLHOP tolerance  
 500 for finding solutions that otherwise may not be found in a center or single point solution.  
 501 The limitations of numerical computation, particularly for a complex environment, are more  
 502 adeptly addressed by accepting some uncertainty in position than by prescribing an exact  
 503 solution. Even though BELLHOP is a greedy estimator for eigenrays, the additional data  
 504 created is a negligible burden.  
 505

506 Underwater navigation research is broadly motivated by acquiring GPS-like navigation  
 507 accuracy in GPS-denied conditions. The Arctic, while remote, is the perfect place to test  
 508 mature navigation technologies in real GPS-denied conditions.

509 Range estimation is an essential step of acoustic localization and navigation. Current  
 510 approaches in real-time underwater acoustic navigation simplify the non-linear relationship  
 511 between a sound speed profile and acoustic propagation with a deterministic sound speed.  
 512 Some post-processing approaches attempt to leverage the acoustic arrival structure via var-  
 513 ious ray methods, but often use a singular SSP for simplicity, even over long term missions  
 514 or dynamic conditions. Thus, the conversion from travel time to range, particularly for  
 515 real-time vehicle deployments, can be pre-conditioned for error growth as the OWTT/range  
 516 increases.

517 For GPS-denied navigation, especially in hostile environments like the Arctic, tolerance  
 518 for error is close to none. This work addresses a critical need in acoustic navigation by

519 retooling acoustic arrival methods generally deemed too complex or labor intensive for real-  
520 time, ray-based range estimation to achieve GPS-like positioning.

521 We hypothesize and validate that the embedded stochastic prediction of a single group  
522 velocity is a smoothly varying function of range, source and receiver depth pairings, as  
523 well as multipath structure. We employ a GPS-tracked experiment to have a ground truth  
524 comparison for real-time localization algorithms. The real-time system achieves GPS-like  
525 navigation for an AUV without taking into account multipath structure; the ranging error  
526 improves by an order of magnitude with the suggested multipath adaptability, minimizing  
527 range error to single meters. Post-processing analysis shows that this method of ranging is  
528 sensitive to GPS drift itself; thus embedding a stochastic prediction of the horizontal group  
529 velocity has an outsized benefit to minimizing trilateration error.

530 There are many avenues through which this approach can be further refined and tested for  
531 field operations. Amongst them is defining the uncertainty grid for BELLHOP via stochastic  
532 or data-driven measures such as the distance traveled by the AUV between ICNN updates  
533 or the magnitude of the position corrections by the ICNN. Another is to entirely remove the  
534 seeded range and instead rely on the submerged asset's depth and recorded OWTT to find  
535 high probability fields in range.

536 The literature in underwater acoustic navigation and positioning is either real-time or  
537 physics-based. In this paper we demonstrate a field-tested approach that is both real-time  
538 and physics-based; this is achieved by coupling data streams with fast acoustic modeling.  
539 The methods exploit the upward refracting nature and the total ice cover of the Arctic  
540 environment to achieve remarkable ranging accuracy and precision. It transforms multipath,

541 widely considered as an obstacle for acoustic ranging, into a new information content to  
 542 refine ranging accuracy. We believe that this work enables more accurate range estimation,  
 543 localization, and/or navigation for any field experiment given known source and receiver  
 544 depths.

545 Performance in other acoustic environments may require introducing a different thresh-  
 546 olded metric to sort time of arrivals. Given the NBC algorithm's improvement with increased  
 547 multipath, its effectiveness is likely only challenged by the valid operational scales of a range  
 548 independent propagation environment. For mesoscale operations, like that of many glid-  
 549 ers, the group velocity criteria may need to be modified to better account for variability  
 550 driven by range dependent propagation through internal waves, eddies, or even bathymetric  
 551 changes like underwater volcanoes. BELLHOP simulations provide other relevant eigenray  
 552 information, like time and angle of arrival, that is ripe for statistical and machine learning  
 553 methods to classify a representative group velocity. A bespoke and fast ray tracing method,  
 554 which was used during ICEX20 to evaluate the acoustic fit of sound speed profile parame-  
 555 terization ([Bhatt et al., 2021](#)), can easily report back the number of turning points instead  
 556 of the number of bounces for multipath classification.

557 This approach will start to break down in extremely dynamic environments. Fast moving  
 558 fronts, as seen in estuaries like the Connecticut River into the Long Island Sound, present  
 559 an entirely new set of challenges not seen by internal waves or eddies. Buoyancy fluctua-  
 560 tions in these regions threaten even simple AUV tasks like following a trackline. Acoustic  
 561 communications are further complicated given a shallow environment with significant scat-  
 562 tering ([Lavery et al., 2010, 2013; Ross and Lavery, 2012](#)), where fast acoustic modeling may

563 only be coherent for trivial probabilities of the ocean state. Realistic *in situ* considerations  
 564 of the acoustic environment may not be possible in such environments without complete  
 565 through-the-sensor integration of echosounder data and/or a hyper-realistic onboard ocean  
 566 model.

567 Many approaches to underwater navigation combine it with acoustic tomography, i.e.,  
 568 a joint estimation of both source and receiver locations and the ocean volume between  
 569 them. There has been considerable success at this effort in post-processing methods,  
 570 which utilize intensive—and due to the non-linearity of sound propagation, often brute  
 571 force—computational methods. For vehicle operations, fast tomography is the ideal im-  
 572 plementation, in that one can fully consider how sound speed structure, horizontally and  
 573 vertically, influences sound propagation. AUVs can serve as moving sources to better image  
 574 the ocean volume ([Deffenbaugh, 1997](#); [Elisseeff \*et al.\*, 2002](#)), where mobile tomography and  
 575 navigation converge on the same set of component technologies: position estimation, sound  
 576 speed parameterization estimation, ray path identification, and vehicle path optimization.

577 But there are overwhelming challenges, operationally and computationally, for fast, mo-  
 578 bile tomography to become a realistic endeavor. Addressing the spatial and temporal scales  
 579 of what can be solved deterministically and what must be solved stochastically imposes a  
 580 resolution constraint on the utility of gridded models—resolving fine features inaccurately  
 581 (or with a false sense of confidence) could be more harmful than assuming range indepen-  
 582 dence. Given that AUV operations are often on small spatial and temporal scales, the added  
 583 benefit of a gridded model is quite small, and in cases like the Arctic, may actually mis-  
 584 characterize the ocean volume. For gliders, with longer and larger operational scales, an

585 ocean model may provide more useful information. Currently gliders are low power and do  
586 not have the storage or computational power to run a full-scale, realistic ocean model. A  
587 lightweight representation of the key environmental and acoustic features, passed through  
588 the same manner of acoustic message from the modem experiment, may drastically improve  
589 glider navigation.

590 **ACKNOWLEDGMENTS**

591 We acknowledge the significant operational effort spearheaded by the LAMSS ICEX20  
 592 team and all our collaborators. Bhatt was funded by a National Defense, Science, and  
 593 Engineering Graduate Fellowship. This work was supported by the Office of Naval Research  
 594 322-OA under ICEX20 (N00014-17-1-2474) and Task Force Ocean (N00014-19-1-2716).

595

596 Ballard, M. S., Badiey, M., Sagers, J. D., Colosi, J. A., Turgut, A., Pecknold, S., Lin, Y.-T.,  
 597 Proshutinsky, A., Krishfield, R., Worcester, P. F., and Dzieciuch, M. A. (2020). “Temporal  
 598 and spatial dependence of a yearlong record of sound propagation from the Canada Basin to  
 599 the Chukchi Shelf,” *The Journal of the Acoustical Society of America* **148**(3), 1663–1680,

600 <http://asa.scitation.org/doi/10.1121/10.0001970>, doi: [10.1121/10.0001970](https://doi.org/10.1121/10.0001970).

601 Barker, L. D. L., Jakuba, M. V., Bowen, A. D., German, C. R., Maksym, T., Mayer, L.,  
 602 Boetius, A., Dutrieux, P., and Whitcomb, L. L. (2020). “Scientific Challenges and Present  
 603 Capabilities in Underwater Robotic Vehicle Design and Navigation for Oceanographic Ex-  
 604 ploration Under-Ice,” *Remote Sensing* **12**(16), 2588, <https://www.mdpi.com/2072-4292/12/16/2588>, doi: [10.3390/rs12162588](https://doi.org/10.3390/rs12162588).

606 Bellingham, J., Leonard, J., Vaganay, J., Goudey, C., Atwood, D., Consi, T., Bales, J.,  
 607 Schmidt, H., and Chryssostomidis, C. (1995). “Auv operations in the arctic,” in *Sea Ice  
 608 Mechanics and Arctic Modeling Workshop*.

- 609 Bhatt, E. C. (2021). “A Virtual Ocean framework for environmentally adaptive, em-  
610 bedded acoustic navigation on autonomous underwater vehicles,” Ph.D. thesis, Mas-  
611 sachusetts Institute of Technology and Woods Hole Oceanographic Institution Joint Pro-  
612 gram, <https://hdl.handle.net/1912/27309>, doi: [10.1575/1912/27309](https://doi.org/10.1575/1912/27309).
- 613 Bhatt, E. C., Howard, B., and Schmidt, H. (2021). “An Embedded Tactical Decision Aid  
614 Framework for Environmentally Adaptive Autonomous Underwater Vehicle Communica-  
615 tion and Navigation,” IEEE Journal of Oceanic Engineering .
- 616 Brooke, J. (1981). “Arcs (autonomous remotely controlled submersible),” in *Proceedings of*  
617 *the 1981 2nd International Symposium on Unmanned Untethered Submersible Technology*,  
618 IEEE, Vol. 2, pp. 28–28.
- 619 Chassignet, E. P., Hurlburt, H. E., Smedstad, O. M., Halliwell, G. R., Hogan, P. J.,  
620 Wallcraft, A. J., Baraille, R., and Bleck, R. (2007). “The HYCOM (HYbrid Coordi-  
621 nate Ocean Model) data assimilative system,” Journal of Marine Systems **65**(1), 60–  
622 83, <https://www.sciencedirect.com/science/article/pii/S0924796306002855>, doi:  
623 [10.1016/j.jmarsys.2005.09.016](https://doi.org/10.1016/j.jmarsys.2005.09.016).
- 624 Chen, R., Poulsen, A., and Schmidt, H. (2019). “Spectral, spatial, and temporal character-  
625 istics of underwater ambient noise in the Beaufort Sea in 1994 and 2016,” The Journal of  
626 the Acoustical Society of America **145**(2), 605–614, [https://asa.scitation.org/doi/  
627 full/10.1121/1.5088601](https://asa.scitation.org/doi/full/10.1121/1.5088601), doi: [10.1121/1.5088601](https://doi.org/10.1121/1.5088601).
- 628 Chen, R., and Schmidt, H. (2020). “Temporal and spatial characteristics of the beaufort  
629 sea ambient noise environment,” The Journal of the Acoustical Society of America **148**(6),  
630 3928–3941.

- 631 Claus, B., Kepper, J. H., Suman, S., and Kinsey, J. C. (2018). “Closed-loop one-way-travel-  
 632 time navigation using low-grade odometry for autonomous underwater vehicles,” Journal of  
 633 Field Robotics **35**(4), 421–434, <https://onlinelibrary.wiley.com/doi/abs/10.1002/rob.21746>, doi: <https://doi.org/10.1002/rob.21746>.
- 634
- 635 Council, N. R. (2011). *National Security Implications of Climate Change for U.S. Naval Forces* (The National Academies Press, Washington, DC), <https://www.nap.edu/catalog/12914/national-security-implications-of-climate-change-for-us-naval-forces>.
- 636
- 637
- 638
- 639 Deffenbaugh, M. (1997). “Optimal Ocean Acoustic Tomography and Navigation with Moving Sources,” PhD Thesis, Massachusetts Institute of Technology.
- 640
- 641 Deffenbaugh, M., Bellingham, J., and Schmidt, H. (1996a). “The relationship between spherical and hyperbolic positioning,” in *OCEANS 96 MTS/IEEE Conference Proceedings. The Coastal Ocean - Prospects for the 21st Century*, Vol. 2, pp. 590–595 vol.2, doi: [10.1109/OCEANS.1996.568293](https://doi.org/10.1109/OCEANS.1996.568293).
- 642
- 643
- 644
- 645 Deffenbaugh, M., Schmidt, H., and Bellingham, J. (1996b). “Acoustic positioning in a fading multipath environment,” in *OCEANS 96 MTS/IEEE Conference Proceedings. The Coastal Ocean - Prospects for the 21st Century*, Vol. 2, pp. 596–600 vol.2, doi: [10.1109/OCEANS.1996.568294](https://doi.org/10.1109/OCEANS.1996.568294).
- 646
- 647
- 648
- 649 Duda, T. F., Morozov, A. K., Howe, B. M., Brown, M. G., Speer, K., Lazarevich, P., Worcester, P. F., and Cornuelle, B. D. (2006). “Evaluation of a Long-Range Joint Acoustic Navigation / Thermometry System,” pp. 1–6, doi: [10.1109/OCEANS.2006.306999](https://doi.org/10.1109/OCEANS.2006.306999).
- 650
- 651

- 652 Duda, T. F., Zhang, W. G., and Lin, Y.-T. (2021). “Effects of Pacific Summer Water  
 653 layer variations and ice cover on Beaufort Sea underwater sound ducting,” Journal of the  
 654 Acoustical Society of America 21.
- 655 Duda, T. F., Zhang, W. G., Lin, Y.-T., and Newhall, A. E. (2019). “Long-range  
 656 sound propagation in the Canada Basin,” in *Underwater Acoustics 2019*, [https://www.  
 657 uaconferences.org/docs/2019\\_papers/UACE2019\\_976\\_Duda.pdf](https://www.uaconferences.org/docs/2019_papers/UACE2019_976_Duda.pdf).
- 658 Elisseeff, P., Schmidt, H., and Xu, W. (2002). “Ocean Acoustic Tomography as a Data  
 659 Assimilation Problem,” IEEE Journal of Oceanic Engineering 27(2), 275–282.
- 660 Eustice, R. M., Whitcomb, L. L., Singh, H., and Grund, M. (2006). “Recent Advances in  
 661 Synchronous-Clock One-Way-Travel-Time Acoustic Navigation,” in *OCEANS 2006*, pp.  
 662 1–6, doi: [10.1109/OCEANS.2006.306931](https://doi.org/10.1109/OCEANS.2006.306931).
- 663 Eustice, R. M., Whitcomb, L. L., Singh, H., and Grund, M. (2007). “Experimental Re-  
 664 sults in Synchronous-Clock One-Way-Travel-Time Acoustic Navigation for Autonomous  
 665 Underwater Vehicles,” in *Proceedings 2007 IEEE International Conference on Robotics  
 666 and Automation*, pp. 4257–4264, doi: [10.1109/ROBOT.2007.364134](https://doi.org/10.1109/ROBOT.2007.364134).
- 667 Fossum, T. O., Norgren, P., Fer, I., Nilsen, F., Koenig, Z. C., and Ludvigsen, M. (2021).  
 668 “Adaptive sampling of surface fronts in the arctic using an autonomous underwater ve-  
 669 hicle,” IEEE Journal of Oceanic Engineering 46(4), 1155–1164, doi: [10.1109/JOE.2021.3070912](https://doi.org/10.1109/JOE.2021.3070912).
- 670
- 671 Freitag, L., Ball, K., Partan, J., Koski, P., and Singh, S. (2015). “Long range acoustic com-  
 672 munications and navigation in the Arctic,” in *OCEANS 2015 - MTS/IEEE Washington*,  
 673 pp. 1–5, doi: [10.23919/OCEANS.2015.7401956](https://doi.org/10.23919/OCEANS.2015.7401956).

- 674 Gardner, A., and Collins, J. (2016). “A second look at Chip Scale Atomic Clocks for long  
675 term precision timing,” OCEANS 2016 MTS/IEEE Monterey doi: [10.1109/OCEANS.2016.7761268](https://doi.org/10.1109/OCEANS.2016.7761268).
- 676
- 677 Graupe, C. E., Van Uffelen, L. J., Webster, S. E., Worcester, P. F., and Dzieciuch, M. A.  
678 (2019). “Preliminary results for glider localization in the beaufort duct using broadband  
679 acoustic sources at long range,” in *OCEANS 2019 MTS/IEEE SEATTLE*, IEEE, pp. 1–6.
- 680 Hayes, D. R., and Morison, J. H. (2002). “Determining turbulent vertical velocity, and  
681 fluxes of heat and salt with an autonomous underwater vehicle,” *Journal of Atmospheric  
682 and Oceanic Technology* **19**(5), 759–779.
- 683 Howe, B. M., Miksis-Olds, J., Rehm, E., Sagen, H., Worcester, P. F., and Haral-  
684 abus, G. (2019). “Observing the Oceans Acoustically,” *Frontiers in Marine Science* **6**,  
685 426, <https://www.frontiersin.org/article/10.3389/fmars.2019.00426/full>, doi:  
686 [10.3389/fmars.2019.00426](https://doi.org/10.3389/fmars.2019.00426).
- 687 Jackson, E. (1983). “Autonomous remotely controlled submersible “ARCS”,” in *Proceedings  
688 of the 1983 3rd International Symposium on Unmanned Untethered Submersible Technol-  
689 ogy*, IEEE, Vol. 3, pp. 77–88.
- 690 Jakuba, M. V., Roman, C. N., Singh, H., Murphy, C., Kunz, C., Willis, C., Sato, T.,  
691 and Sohn, R. A. (2008). “Long-baseline acoustic navigation for under-ice autonomous  
692 underwater vehicle operations,” *Journal of Field Robotics* **25**(11-12), 861–879.
- 693 Kepper, J. H., Claus, B. C., and Kinsey, J. C. (2017). “MEMS IMU and One-Way-Travel-  
694 Time Navigation for Autonomous Underwater Vehicles,” in *Oceans 2017 - Aberdeen*, Ab-  
695 erdeen, UK.

- 696 Krishfield, R., Toole, J., Proshutinsky, A., and Timmermans, M.-L. (2008). “Automated  
 697 ice-tethered profilers for seawater observations under pack ice in all seasons,” *Journal of*  
 698 *Atmospheric and Oceanic Technology* **25**(11), 2091–2105.
- 699 Kukulya, A., Plueddemann, A., Austin, T., Stokey, R., Purcell, M., Allen, B., Littlefield, R.,  
 700 Freitag, L., Koski, P., Gallimore, E. *et al.* (2010). “Under-ice operations with a remus-100  
 701 auv in the arctic,” in *2010 IEEE/OES Autonomous Underwater Vehicles*, IEEE, pp. 1–8.
- 702 Kunz, C., Murphy, C., Camilli, R., Singh, H., Bailey, J., Eustice, R., Jakuba, M., Nakamura,  
 703 K.-i., Roman, C., Sato, T., Sohn, R. A., and Willis, C. (2008a). “Deep sea  
 704 underwater robotic exploration in the ice-covered Arctic ocean with AUVs,” in *2008*  
 705 *IEEE/RSJ International Conference on Intelligent Robots and Systems*, pp. 3654–3660,  
 706 doi: [10.1109/IROS.2008.4651097](https://doi.org/10.1109/IROS.2008.4651097).
- 707 Kunz, C., Murphy, C., Camilli, R., Singh, H., Bailey, J., Eustice, R., Jakuba, M., Nakamura,  
 708 K.-i., Roman, C., Sato, T. *et al.* (2008b). “Deep sea underwater robotic exploration in  
 709 the ice-covered arctic ocean with AUVs,” in *2008 IEEE/RSJ International Conference on*  
 710 *Intelligent Robots and Systems*, IEEE, pp. 3654–3660.
- 711 Lavery, A. C., Chu, D., and Moum, J. N. (2010). “Measurements of acoustic scattering from  
 712 zooplankton and oceanic microstructure using a broadband echosounder,” *ICES Journal*  
 713 of Marine Science **67**(2), 379–394, doi: [10.1093/icesjms/fsp242](https://doi.org/10.1093/icesjms/fsp242).
- 714 Lavery, A. C., Geyer, W. R., and Scully, M. E. (2013). “Broadband acoustic quan-  
 715 tification of stratified turbulence,” *The Journal of the Acoustical Society of Amer-*  
 716 *ica* **134**(1), 40–54, <http://scitation.aip.org/content/asa/journal/jasa/134/1/10.1121/1.4807780>, doi: [10.1121/1.4807780](https://doi.org/10.1121/1.4807780).

- 718 Light, R., and Morison, J. (1989). “The autonomous conductivity-temperture vehicle: First  
 719 in the seashuttle family of autonomous underwater vehicle’s for scientific payloads,” in  
 720 *Proceedings OCEANS*, Vol. 3, pp. 793–798, doi: [10.1109/OCEANS.1989.586683](https://doi.org/10.1109/OCEANS.1989.586683).
- 721 Litvak, A. (2015). “Acoustics of the deepwater part of the arctic ocean and of russia’s  
 722 arctic shelf,” *Herald of the Russian Academy of Sciences* **85**, 239–250, doi: [10.1134/S1019331615030144](https://doi.org/10.1134/S1019331615030144).
- 724 Mikhalevsky, P. N., Sperry, B. J., Woolfe, K. F., Dzieciuch, M. A., and Worcester, P. F.  
 725 (2020). “Deep ocean long range underwater navigation,” *The Journal of the Acoustical  
 726 Society of America* **147**(4), 2365–2382, <http://asa.scitation.org/doi/10.1121/10.0001081>, doi: [10.1121/10.0001081](https://doi.org/10.1121/10.0001081).
- 727 Norgren, P., Lubbad, R., and Skjetne, R. (2014). “Unmanned underwater vehicles in Arctic  
 729 operations,” p. 14.
- 730 Paull, L., Saeedi, S., Seto, M., and Li, H. (2014). “AUV Navigation and Localization:  
 731 A Review,” *IEEE Journal of Oceanic Engineering* **39**(1), 131–149, <http://ieeexplore.ieee.org/document/6678293/>, doi: [10.1109/JOE.2013.2278891](https://doi.org/10.1109/JOE.2013.2278891).
- 733 Plueddemann, A. J., Kukulya, A. L., Stokey, R., and Freitag, L. (2012). “Autonomous  
 734 Underwater Vehicle Operations Beneath Coastal Sea Ice,” *IEEE/ASME Transactions  
 735 on Mechatronics* **17**(1), 54–64, doi: [10.1109/TMECH.2011.2174798](https://doi.org/10.1109/TMECH.2011.2174798) conference Name:  
 736 IEEE/ASME Transactions on Mechatronics.
- 737 Porter, M. B. (2011). “The BELLHOP Manual and User’s Guide (Preliminary Draft),”  
 738 1–57, <http://esme.bu.edu/data/papers/HLS-2010-1.pdf>.

- 739 Poulsen, A. J., and Schmidt, H. (2016a). “Acoustic noise properties in the rapidly changing  
740 Arctic Ocean,” Buenos Aires, Argentina, p. 070005, <http://asa.scitation.org/doi/abs/10.1121/2.0000552>, doi: [10.1121/2.0000552](https://doi.org/10.1121/2.0000552).
- 742 Poulsen, A. J., and Schmidt, H. (2016b). “Acoustic noise properties in the rapidly changing  
743 arctic ocean,” in *Proceedings of Meetings on Acoustics*, Acoustical Society of America, Vol.  
744 28, p. 070005.
- 745 Randeni, S., Schneider, T., and Schmidt, H. (2020). “Construction of a high-resolution  
746 under-ice AUV navigation framework using a multidisciplinary virtual environment,” in  
747 *2020 IEEE/OES Autonomous Underwater Vehicles Symposium (AUV)*, pp. 1–7, doi: [10.1109/AUV50043.2020.9267950](https://doi.org/10.1109/AUV50043.2020.9267950).
- 748 Randeni, S., Schneider, T., Schmidt, H., Bhatt, E., and Viquez, O. (2021). “A high-  
749 resolution AUV navigation framework with integrated communication and tracking for  
750 under-ice deployments,” *Field Robotics* (in review).
- 751 Ross, T., and Lavery, A. C. (2012). “Acoustic scattering from density and sound speed  
752 gradients: modeling of oceanic pycnoclines.” *The Journal of the Acoustical Society of  
753 America* **131**(1), EL54–9, <http://www.ncbi.nlm.nih.gov/pubmed/22280730>, doi: [10.1121/1.3669394](https://doi.org/10.1121/1.3669394).
- 755 Rossby, T., Dorson, D., and Fontaine, J. (1986). “The RAFOS System,” *Journal of Atmo-  
756 spheric and Oceanic Technology* **3**(4), 672–679, [https://journals.ametsoc.org/view/journals/atot/3/4/1520-0426\\_1986\\_003\\_0672\\_trs\\_2\\_0\\_co\\_2.xml](https://journals.ametsoc.org/view/journals/atot/3/4/1520-0426_1986_003_0672_trs_2_0_co_2.xml), doi: [10.1175/1520-0426\(1986\)003<0672:TRS>2.0.CO;2](https://doi.org/10.1175/1520-0426(1986)003<0672:TRS>2.0.CO;2).

- 760 Schmidt, H., and Schneider, T. (2016). “Acoustic communication and navigation in the  
 761 new arctic—a model case for environmental adaptation,” in *2016 IEEE Third Underwater  
 762 Communications and Networking Conference (UComms)*, IEEE, pp. 1–4.
- 763 Schneider, T., and Schmidt, H. (2018). “NETSIM: A Realtime Virtual Ocean Hardware-  
 764 in-the-loop Acoustic Modem Network Simulator,” in *2018 Fourth Underwater Commu-  
 765 nications and Networking Conference (UComms)*, pp. 1–5, doi: [10.1109/UComms.2018.8493188](https://doi.org/10.1109/UComms.2018.8493188).
- 766 Schneider, T., Schmidt, H., and Randeni, S. (2020). “Self-Adapting Under-Ice Integrated  
 767 Communications and Navigation Network,” in *Underwater Communications*, p. 5.
- 768 Singh, S., Grund, M., Bingham, B., Eustice, R., Singh, H., and Freitag, L. (2006). “Under-  
 769 water Acoustic Navigation with the WHOI Micro-Modem,” in *OCEANS 2006*, IEEE,  
 770 Boston, MA, USA, pp. 1–4, <http://ieeexplore.ieee.org/document/4099008/>, doi:  
 771 [10.1109/OCEANS.2006.306853](https://doi.org/10.1109/OCEANS.2006.306853).
- 772 Timmermans, M.-L., and Winsor, P. (2013). “Scales of horizontal density structure in the  
 773 chukchi sea surface layer,” *Continental Shelf Research* **52**, 39–45.
- 774 Toole, J. M., Krishfield, R. A., Timmermans, M.-L., and Proshutinsky, A. (2011). “The  
 775 ice-tethered profiler: Argo of the arctic,” *Oceanography* **24**(3), 126–135.
- 776 Van Uffelen, L. J., Howe, B. M., Nosal, E.-M., Carter, G. S., Worcester, P. F., and Dzieciuch,  
 777 M. A. (2016). “Localization and Subsurface Position Error Estimation of Gliders Using  
 778 Broadband Acoustic Signals at Long Range,” *IEEE Journal of Oceanic Engineering* **41**(3),  
 779 501–508, doi: [10.1109/JOE.2015.2479016](https://doi.org/10.1109/JOE.2015.2479016).

- 781 Van Uffelen, L. J., Nosal, E.-M., Howe, B. M., Carter, G. S., Worcester, P. F., Dzieci-  
782 uch, M. A., Heaney, K. D., Campbell, R. L., and Cross, P. S. (2013). “Estimating  
783 uncertainty in subsurface glider position using transmissions from fixed acoustic tomog-  
784 raphy sources,” *The Journal of the Acoustical Society of America* **134**(4), 3260–3271,  
785 <https://asa.scitation.org/doi/full/10.1121/1.4818841>, doi: [10.1121/1.4818841](https://doi.org/10.1121/1.4818841).
- 786 Van Uffelen, L. J. V. (2021). “Global Positioning Systems: Over Land and Under Sea,”  
787 *Acoustics Today* **17**(1), 9.
- 788 Webster, S. E., Eustice, R. M., Singh, H., and Whitcomb, L. L. (2009). “Preliminary  
789 deep water results in single-beacon one-way-travel-time acoustic navigation for underwater  
790 vehicles,” *2009 IEEE/RSJ International Conference on Intelligent Robots and Systems,*  
791 IROS 2009 2053–2060, doi: [10.1109/IROS.2009.5354457](https://doi.org/10.1109/IROS.2009.5354457).
- 792 Webster, S. E., Eustice, R. M., Singh, H., and Whitcomb, L. L. (2012). “Advances in  
793 single-beacon one-way-travel-time acoustic navigation for underwater vehicles,” *The In-*  
794 *ternational Journal of Robotics Research* **31**(8), 935–950, <https://doi.org/10.1177/0278364912446166>, doi: [10.1177/0278364912446166](https://doi.org/10.1177/0278364912446166).
- 795 Webster, S. E., Freitag, L. E., Lee, C. M., and Gobat, J. I. (2015). “Towards real-time under-  
796 ice acoustic navigation at mesoscale ranges,” in *2015 IEEE International Conference on*  
797 *Robotics and Automation (ICRA)*, IEEE, pp. 537–544.
- 798 Wu, L., Yang, X.-Y., and Hu, J. (2018). “Assessment of Arctic sea ice simulations  
799 in CMIP5 models,” *The Cryosphere* <https://doi.org/10.5194/tc-2018-26>, doi: [10.](https://doi.org/10.5194/tc-2018-26)  
800 [5194/tc-2018-26](https://doi.org/10.5194/tc-2018-26).